Morphological improvement of CH₃NH₃PbI₃ films using blended solvents for perovskite solar cells

Nam Le, Nguyen Tam Nguyen Truong, Trang Le, Mohan Reddy Pallavolu, Hye Jun Jeon, and Chinho Park†

School of Chemical Engineering, Yeungnam University, 280 Daehak-ro, Gyeongsan 38541, Korea

Abstract−Perovskite solar cells with the structure of glass/florine-doped tin oxide (FTO)/electron transfer layer (ETL)/perovskite/hole transfer layer (HTL)/Ag were fabricated. The effects of blending solvents and thermal annealing on the surface morphology, structural, and optical properties of perovskite (CH₃NH₃PbI₃) active layer were investigated. The active layer was optimized by adding 2-butanol (2-BTA) as an eco-friendly solvent into methyl ammonium iodide (MAI) solution used for spin coating on PbI₂/(dimethylformamide (DMF)+dimethyl sulfoxide (DMSO)) film in the second step. The resulting morphology of CH₃NH₃PbI₃ films was smooth and pinholes in the films were also reduced without change in the structure. The effects of thermal annealing on the surface morphology and structural properties of active layer were also studied. The fabricated device for the optimized condition showed the maximum power conversion efficiency (PCE) of ~8.6%.

Keywords: Perovskite, Solar Cell, Optical, Morphological, Structural, Thermal Annealing

INTRODUCTION

Perovskite solar cells (PSCs) have become one of the most potential photoelectric conversion devices for inexpensive and high photovoltaic conversion efficiency (PCE) [1,2]. Perovskites have unique properties such as suitable band gap, excellent light-harvesting properties, broad-spectrum absorption range and sufficient carrier mobility [3-7]. Moreover, abundance of the materials, along with the low-cost in processing and the efficiency of the devices have made PSCs become one of the most promising photovoltaic cells to enter into the market [8]. PCS can also be combined with photoelectrochemical cells to simultaneously produce green hydrogen. The first significant perovskite solar cell was made by Miyasaka and co-workers, who reported an efficiency of 3.81% in 2009 [9]. Recently, perovskite-silicon tandem cells with 25.7% efficiency were fabricated by King Abdullah University of Science and Technology (KAUST) and University of Toronto team [10].

The most efficient perovskite material for the photovoltaic application to date is methylammonium lead trihalide (CH₃NH₃PbX₃). Various techniques such as spin coating [11], dip coating [12], vapor deposition [13,14], spray coating [15] and inkjet printing [16] have been used to develop high-quality perovskite thin-films. Among them, a spin coating method is widely used due to the low-cost and ease in the processing. The spin-coating used for the perovskite solar cells is typically divided into one-step and sequential two-step methods [17]. In one-step method, both inorganic (e.g., PbX₂, X=Cl, Br, I) and organic (e.g., methylamine iodide (MAI)) materials are included and dissolved in the same solution using polar organic solvents (e.g., γ-butyrolactone, dimethylformamide (DMF), dimethyl sulfoxide (DMSO)) or a mixture of them to form the precursor solution [18-20]. The precursor solution is then spin-coated or drop-casted on the prepared substrate. However, the problem of poor coverage of perovskite thin film has been an issue due to the fast crystallization of perovskite materials [21]. To solve this problem, two-step deposition was introduced, resulting in a denser and smoother perovskite thin film [21,22]. In this method, a lead (II) iodide (PbI₂) precursor solution is spin-coated on the substrate, and post-conversion to perovskite (CH₃NH₃PbI₃) by reacting with a methyl ammonium iodide (MAI) solution [23]. However, the main problems of two sequential steps is the incomplete conversion of PbI₂ to perovskite and rough surface structure of perovskite thin films [24,25]. Hence, much effort has been undertaken to improve perovskite film quality by introducing additives during the fabrication process. For instance, Li et al. fabricated high-quality planar perovskites film via HCl accelerated formation by adding 33 wt% hydrochloric acid (HCl) to the lead (II) iodide PbI₂ [26]. In 2015, 4-tert-butylpyridine (TBP) was used as an additive into the PbI₂ solution to achieve uniform and pin-holes-free perovskite thin films [27]. Also, 1-chloronaphthalene was introduced in the precursor solution to enhance the perovskite film quality and it was observed that the PCE of the devices was significantly improved (9.46%) [28]. More recently, Su et al. investigated a significant enhancement of PCE (17.21%) in the PSCs via adding trimesic acid (TMA) additive into the PbI₂ solution by a two-step method [29]. Although many research groups have paid attention to the additives into PbI₂, few reports were focusing on additives into MAI solution [30,31]. In addition, the additives into MAI solution, such as iodide (I₂) and methyl ammonium chloride (MACl) may remain in the films after fabrication, which can change the properties of the films.

In this research, 2-butanol (2-BTA) was first used as an additive into MAI solution to grow perovskite film by the typical sequential deposition for preparing high-quality perovskite films. The improve-

ment in the $CH_3NH_3PbI_3$ thin film quality indicates that the additives to MAI are as important as additives to PbI_2 solution on the morphology of perovskite film. Due to the less polarity of 2-butanol (2-BTA), leading to increasing the reaction time, the additive significantly improved the quality of perovskite films and reproducibility of the experiment. Moreover, 2-BTA is an environmentally friendly solvent that can be removed easily from the films after annealing without changing the properties of the films, which ensures the purity of perovskite thin films. A device with the structure of FTO/ZnO/perovskite/spiro-OMETAD/Ag was fabricated and characterized.

EXPERIMENTAL DETAILS

1. Materials

All chemicals, methylamonium iodide (MAI, 99.5%), acetonitrile (CH_3CN, 99.5%), 2-propanol (C_3H_8O, 99.5%), 2-butanol ($C_4H_{10}O$, 99.5%), zinc powder, Lead(II) iodide (PbI_2, 99%), Lithium bis(trifluoromethanesulfonyl)imide (LiTFSI, 98%), and 4-tert-butylpyridine (tBP, 98%), were products from Sigma Aldrich and used without any further purification.

2. Device Fabrication

2-1. The Electron Transport Layer (ZnO) Solution Preparation

The electron transfer layer solution was prepared by dissolving $Zn(CH_3CO_2)_2 \cdot 2H_2O$, in 0.2 mL ethanolamine, 4.8 mL 2-methoxyethanol and stirring overnight.

2-2. The PbI_2 Solution

The PbI_2 solution was prepared by dissolving 924 mg PbI_2 with a mixed solvent (DMF : DMSO=9 : 1) and stirring at 100 °C for 24 hr.

2-3. MAI Solution

The different MAI solutions (8 mg/mL) were prepared by changing the volume ratio (vol%) of 2-BTA in the mixture solvent of (IPN+2-BTA) solution (0%, 5%, 25%, 50%, 100%).

2-4. The Hole Transfer Layer (HTM) Layer

The hole transfer layer solution was prepared by dissolving Spiro-MeOTAD (0.068 M), LiTFSI (0.018 M) and tBP (0.05 M) in the 1 mL mixed solvent of chlorobenzene and acetonitrile.

2-5. Device Fabrication

The fluorine-doped tin oxide (FTO) substrates were ultrasonicated sequentially with acetone, isopropanol and deionized water for 10 min of each and dried by nitrogen gun. The ETL layer was deposited on the top of Glass/FTO substrate at 3,000 rpm for 30 s and heated at 250 °C for 15 min on a hotplate. PbI_2 solution was spin-coated at 6,000 rpm for 30 s, then annealed at 60 °C for 15 min and then annealed at 100 °C for 45 min to form the PbI_2 films. Then, the MAI solutions with different volume ratio (vol%) of 2-BTA in the mixture solvent of (IPA+2-BTA) were spin-coated on top of FTO/ZnO/PbI_2 film at 4,000 rpm for 20 s to form perovskite structure. The HTL was spin-coated on top of the perovskite films at 3,000 rpm for 30 s. Finally, Ag (~120 nm) was deposited on the top of perovskite film by using E-beam thermal evaporation to form Glass/FTO/ZnO/Perovskite/Spiro-MeOTAD/Ag structure, as shown in Fig. 1.

3. Characterizations

The structural properties of perovskite thin films were measured by X-ray diffraction (XRD, PANalytical, X'Pert-PRO) with 3 kW
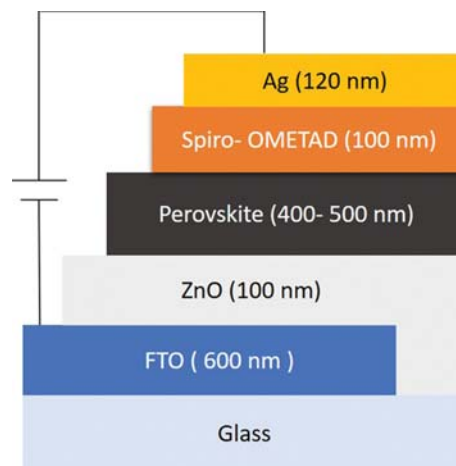
Fig. 1. Schematic diagram of the device structure.

X-ray generator. The surface morphology and surface roughness of perovskite films were carried out by scanning electron microscopy (SEM, Hitachi S-4800) and atomic force microscopes (AFM, XE-100 Park system). The transmittance spectra of perovskite films were characterized by UV-Vis spectrophotometer (Cary 5000, Varian) in the wavelength range from 200 to 1,800 nm. The PL characteristics of $CH_3NH_3PbI_3$ thin films were examined by the photoluminescence spectrometer. The device's power conversion efficiency (PCE) was measured under simulated solar radiation, 100 mW/cm², 400 V (Keithley model 2400 Source).

RESULTS AND DISCUSSION

1. Effects of Blending Solvent on the Structural, Morphological, and Optical Properties of Perovskite Thin-films

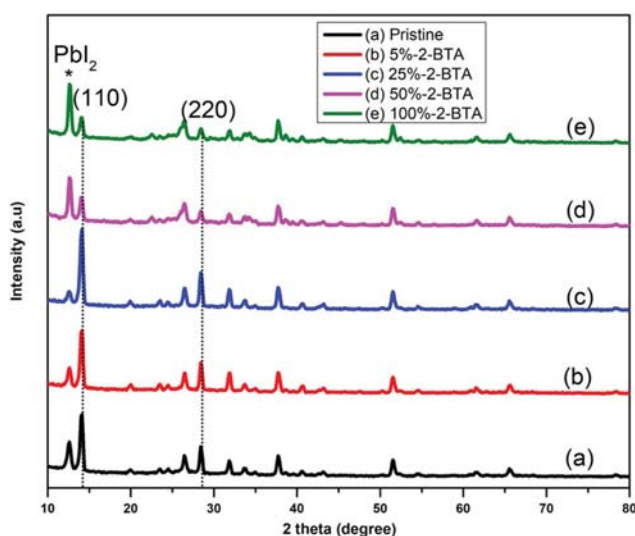Fig. 2 shows the XRD patterns of perovskite films, which con-

Fig. 2. X-ray diffraction (XRD) patterns of pure (a) IPA, (b) 5%, (c) 25%, (d) 50% 2-BTA and (e) pure 2-BTA based $CH_3NH_3PbI_3$ films.

firms the role of additive 2-BTA on the crystallization of perovskite films. All the films have a high intensity of diffraction peaks located at 14.14° and 28.43° corresponding to the (110) and (220) major planes of perovskite thin-films, respectively [32]. Besides, an impurity diffraction peak at 12.6° indicates the existence of PbI_2 demonstrating the incomplete conversion from PbI_2 to $MAPbI_3$, which can reduce the PCE of the solar cells [33]. When the volume ratio (%) of 2-BTA in blending solvent increases to 5 vol% and 25 vol%,

the intensity of peak $MAPbI_3$ increases, whereas the intensity of impurity peak PbI_2 (at 12.8°) is quenched. But when the ratio of 2-BTA in the mixed solvent increases to more than 50 vol%, the intensity of the PbI_2 peak increases dramatically. This may be due to the retarding crystallization process that will be discussed in the following section.

SEM and AFM were used to evaluate the effect of additive 2-BTA volume ratio (vol%) on the coverage and roughness of per-
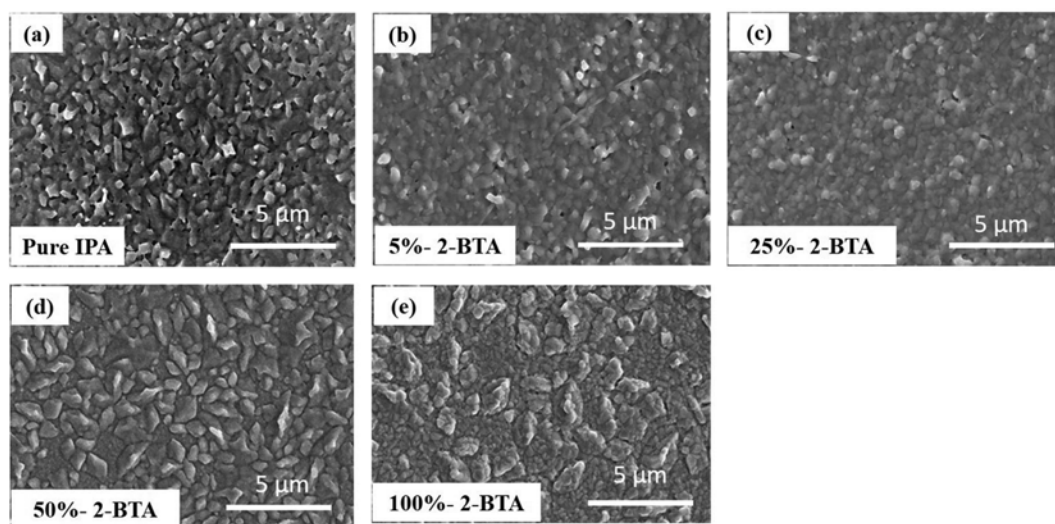

Fig. 3. SEM images of perovskite films processed by MAI dissolved in IPA/2-BTA mixed solvent containing 0, 5, 25, 50 and 100% 2-BTA (scale bar: 5 μm).
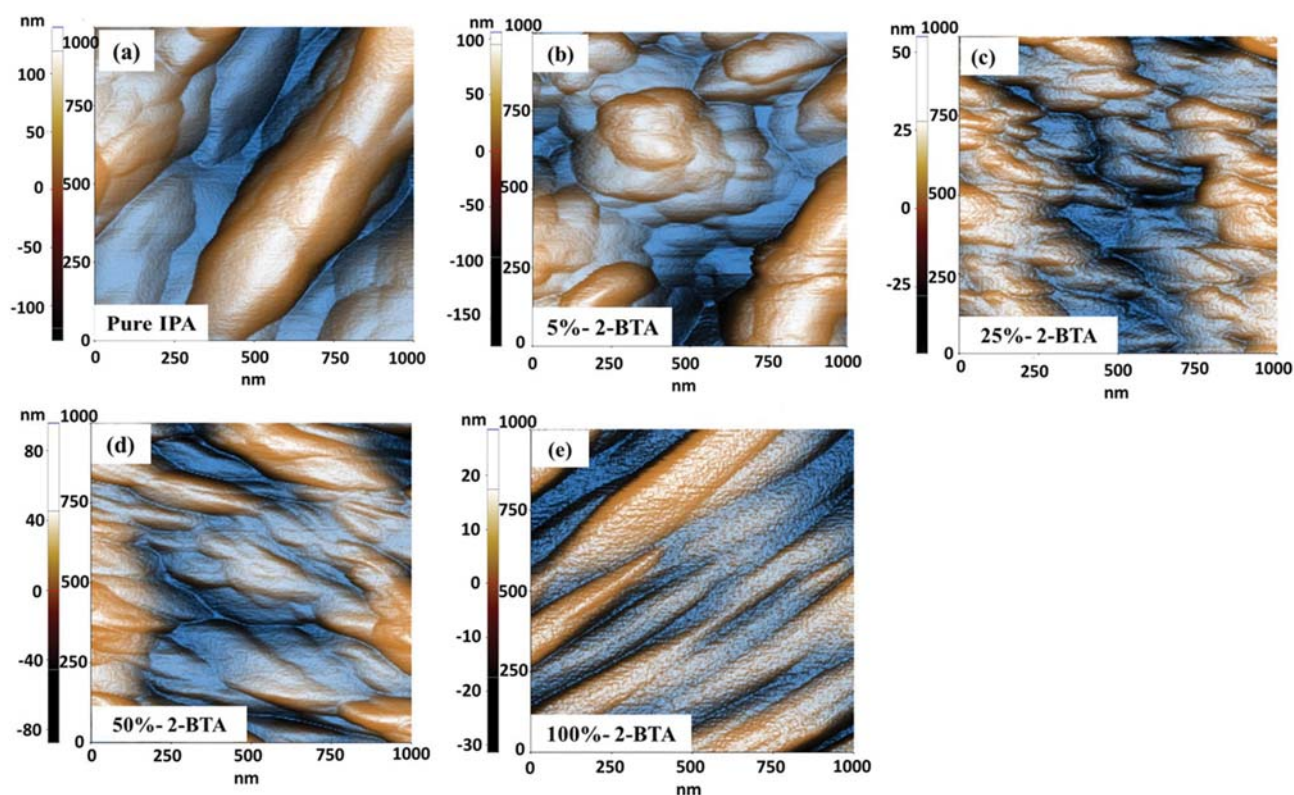

Fig. 4. 2D AFM images of perovskite films processed by MAI dissolved in IPA/2-BTA mixed solvent containing 0, 5, 25, 50 and 100% 2- BTA.

Table 1. Roughness analysis of the AFM images

	Root mean square (nm)
Pristine	~36
2-BTA vol.5%	~15
2-BTA vol.25%	~6
2-BTA vol. 50%	~13
2-BTA vol.100%	~195

ovskite films. As shown in Fig. 3(a), the pristine perovskite films without 2-BTA additive had many pin-holes and voids. The discontinuous and low surface coverage led to poor charge transport and insufficient light-harvesting in perovskite films [7,21]. By adding 2-BTA 25 vol%, the films with 2-BTA (25 vol%) became more uniform and presented much better coverage as shown in Fig. 3(c). However, when the concentration of 2-BTA increased more than 25 vol% as shown in Fig. 3(d), (e), the film surface morphology became worse because many voids were produced between the grains with the low surface coverage of $CH_3NH_3PbI_3$ thin films, leading to increase in the recombination of carriers [7].
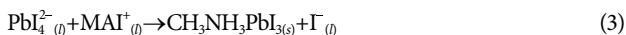
Effects of 2-BTA additive on the perovskite film's surface roughness were measured by AFM, as shown in Fig. 4 and the root mean square (RMS) values were tabulated in Table 1. From Table 1, the pristine film produced without additive has high roughness with an RMS of ~36 nm, while the films produced with 2-BTA additive have lower roughness except for the film with 100% 2-BTA additive. In addition, the film with 25% 2-BTA additive has very low roughness (~6 nm), which indicates that a mixed solvent containing 25% 2-BTA additive is good for perovskite thin films preparation.

The improved quality of perovskite film might be explained in detail. In this research, perovskite active layers were prepared by the 2-step method following the two mechanisms.
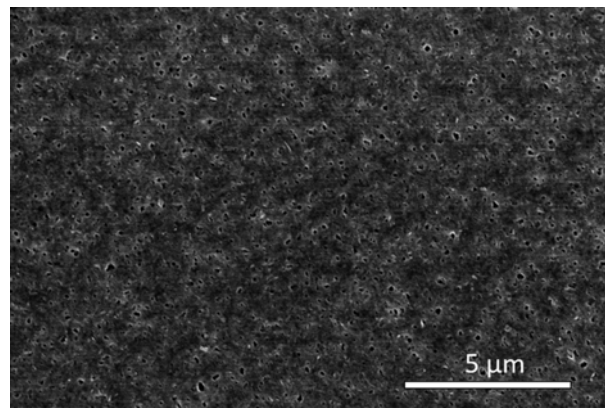
In situ intercalation:
$$PbI_{2(s)}+MAI_{(l)}{\rightarrow}CH_3NH_3PbI_{3(s)} \tag{1}$$

Dissolution- recrystallization:
$$PbI_{2(l)}+2I^-_{(l)}{\rightarrow}PbI_4^{2-}{}_{(l)} \tag{2}$$

$$PbI_4^{2-}{}_{(l)}+MAI^+_{(l)}{\rightarrow}CH_3NH_3PbI_{3(s)}+I^-_{(l)} \tag{3}$$

The crystal growth of perovskite thin films can be classified into two types: *in situ* intercalation (1) and dissolution-recrystallization (2), (3) [34]. At a low MAI concentration, the reaction follows *in situ* intercalation but PbI_2 cannot convert completely to $CH_3NH_3PbI_3$ due to the lack of MAI [35]. To push the reaction (1) forward, a higher MAI concentration can be used, but reactions (2) and (3) also can happen. So, the formation of perovskite films will follow the dissolution-crystallization mechanism, leading to decrease in the uniformity of the films [35]. In this research, the use of low polarity solvent and larger molecular such as 2-BTA allowed perovskite thin films to grow via the *in situ* intercalation mechanism than the dissolution-crystallization when using IPA. It can be observed that low polarity solvent does not favor the dissolution of PbI_2 and suppresses reactions (2) and (3). With *in situ* intercalation, the $CH_3NH_3PbI_3$ grains grow *in situ* to fill the void between the PbI_2 molecules (Fig. 5) and maintain the parallel geometries of PbI_2 framework, resulting in dense and high coverage perovskite

Fig. 5. SEM image of PbI$_2$ thin-film (scale bar: 5 μm).

thin-films. Thus, *in situ* intercalation retards the crystallization process and reduces the voids in the films by the gradual expansion of crystals. But when total IPA was changed by 100% 2-BTA the film had a high roughness and many pin holes. This may be explained by the higher boiling point of 2-BTA solvent, that needs higher annealing temperature and longer annealing time. We should remember that at high temperature and longer annealing time the perovskite thin-films can be decomposed to PbI_2 and MAI, which can be confirmed by the high intensity of impurity PbI_2 peak from XRD result. From XRD, SEM and AFM, we chose 25 vol% additive 2-BTA as the best condition to prepare the perovskite thin-films.

To further understand the effect of 2-BTA additive on the perovskite films, we carried out ultraviolet-visible absorption spectroscopy. All the perovskite thin-films showed a strong absorption over the whole UV-VIS range with an absorption band edge at 760 nm as shown in Fig. 6. We observed significant differences in the change of normalized absorbance for the pristine without additive and modified samples with 2-BTA additive. The higher absorption of the films with 5 vol% and 25 vol% of 2-BTA addition indicates the higher
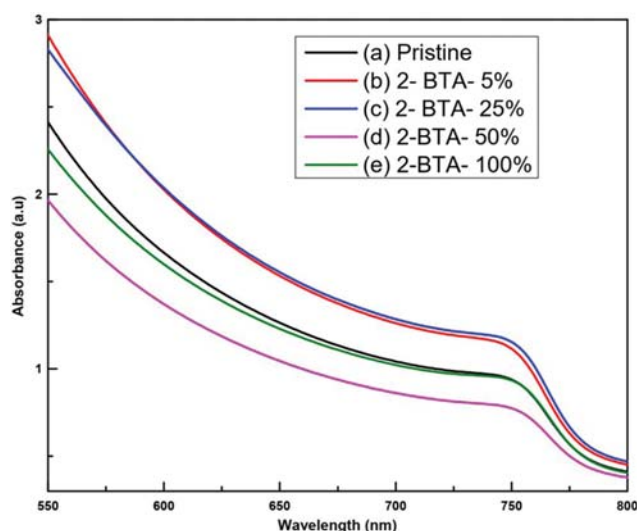
Fig. 6. UV-vis absorption spectra of (a) pure IPA, (b) 5% BTA, (c) 25% BTA, (d) 50% BTA and (e) 100% 2-BTA based CH$_3$NH$_3$PbI$_3$ perovskite films on FTO substrates.
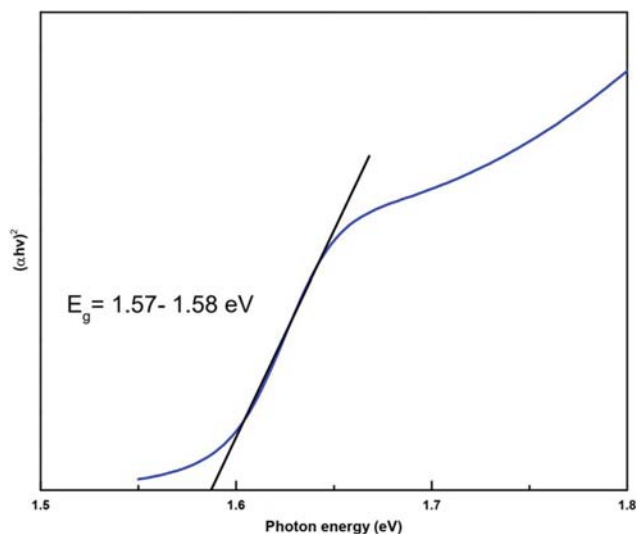
Fig. 7. The plot of $(\alpha h\nu)^2$ versus photon energy hν of perovskite film by MAI dissolved in IPN/2-BTA mixed solvent containing 25% of 2-BTA.

Fig. 9. Current density-voltage (J-V) curves of perovskite films processed by MAI dissolved in IPA/2-BTA mixed solvent containing 0, 5, 25, 50 and 100% 2-BTA.

Table 2. Photovoltaic current-voltage parameters of perovskite solar cells at different additive ratio of 2-BTA

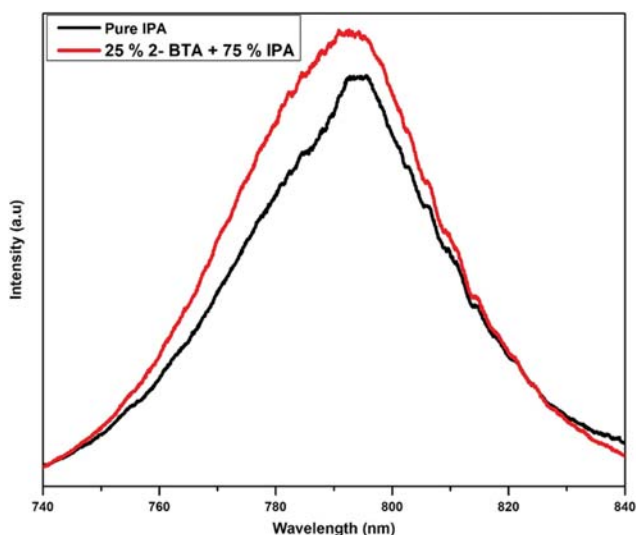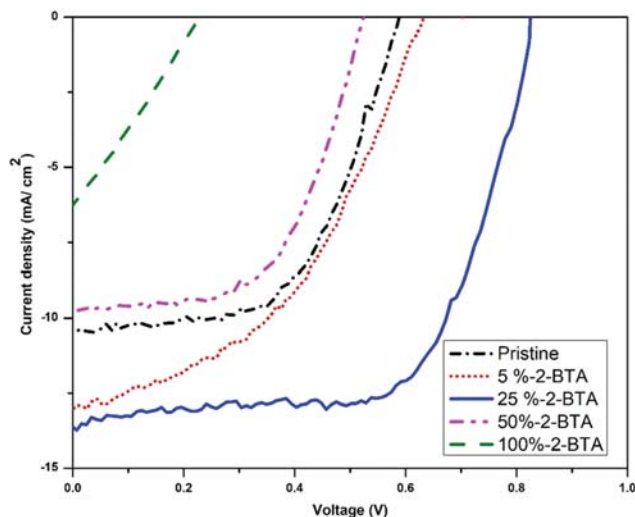| Samples	V_{oc} (V)	J_{sc} (mA/cm^2)	FF (%)	PCE (%)
Pristine	0.59	10.40	57.0	3.5
2-BTA vol.5%	0.62	13.02	44.6	3.7
2-BTA vol.25%	0.82	13.08	64.5	6.9
2-BTA vol. 50%	0.52	9.74	57.7	2.9
2-BTA vol.100%	0.23	6.26	29.1	0.4

Fig. 8. Steady-state photoluminescence (PL) of perovskite thin films prepared with pure IPA and 25% additive 2-BTA+75% IPA.

crystallinity of perovskite corresponding to the XRD results. The higher absorption led to improving of the device's current density. Additionally, the bandgap energy E$_g$ was calculated according to the following equation: $\alpha h\nu = A(h\nu - E_g)^{1/2}$, where E$_g$ is the band gap energy, A is a constant, hv is the photon energy, α is the absorption coefficient [36]. The E$_g$ of additive 2-BTA 25 vol% perovskite film is about 1.58 eV, as shown in Fig. 7, which matches with the E$_g$ of perovskite thin film.

The effects of 2-BTA additive solvent on the optical property of perovskite film were also studied by measuring the steady-state photoluminescence. Fig. 8 shows the PL spectrum of perovskite film without and with 25 vol% of 2-BTA additive exhibits emission peaks located at around 790 nm, which matches with the previous reports [37]. However, we also observed that the peak inten-

sity of perovskite film with 25 vol% 2-BTA additive is higher than that of the perovskite film without 2-BTA additive. The higher intensity of perovskite film demonstrates higher crystallinity and better morphology of the film with 2-BTA additive. This can mainly be ascribed to the fact that the number of crystal defects induced is decreased, so non-radiative recombination paths are reduced by the 2-BTA addition. The decrease of defects is beneficial to improving V$_{oc}$, J$_{sc}$ and the FF as well as PCE.

PVSCs based perovskite films without and with 2-BTA additive were fabricated. The performance of the fabricated device (shown in Fig. 9) was tested with the device parameters such as J$_{sc}$, V$_{oc}$, FF, and PCE as shown in Table 2. The pristine device without 2-BTA additive shows a PCE is about 3.5% (J$_{sc}$ ~10.40 mA/cm^2; V$_{oc}$ ~0.59 V; FF ~57.0%). Therefore, the device with 25 vol% of 2-BTA additive shows a PCE of about 6.9% (J$_{sc}$ ~13.08 mA/cm^2; V$_{oc}$ ~0.82 V; FF ~64.5%). The efficiency of the device with 2-BTA additive was increased about twice compared with the device without 2-BTA additive due to the higher crystallinity and lower defect states in the perovskite films.

2. Effects of Thermal Annealing on the Structural and Morphological Properties of Perovskite Thin-films

Three different annealing processes were performed for perovskite thin films, as shown in Fig. 10. Fig. 10(a) shows the first annealing process; the films were annealed in two steps (at 60 °C/ 15 min and then 100 °C/45 min). Fig. 10(b) shows the second anneal-
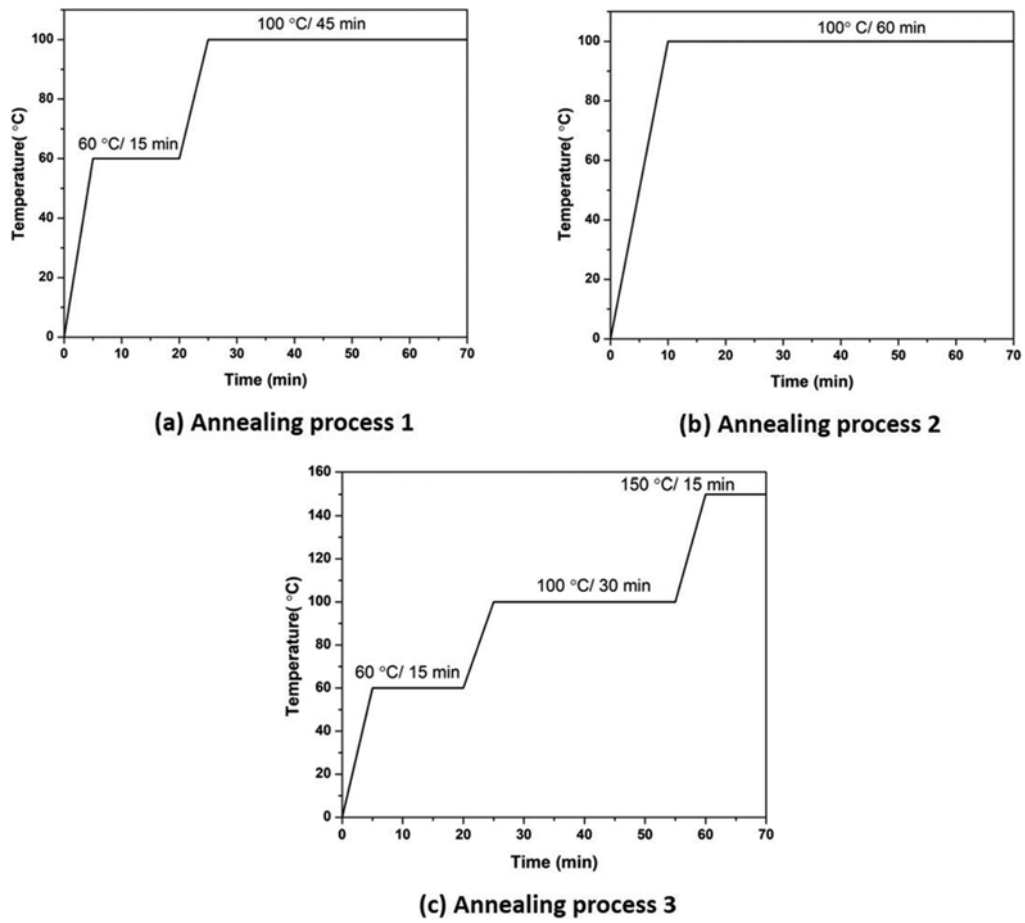
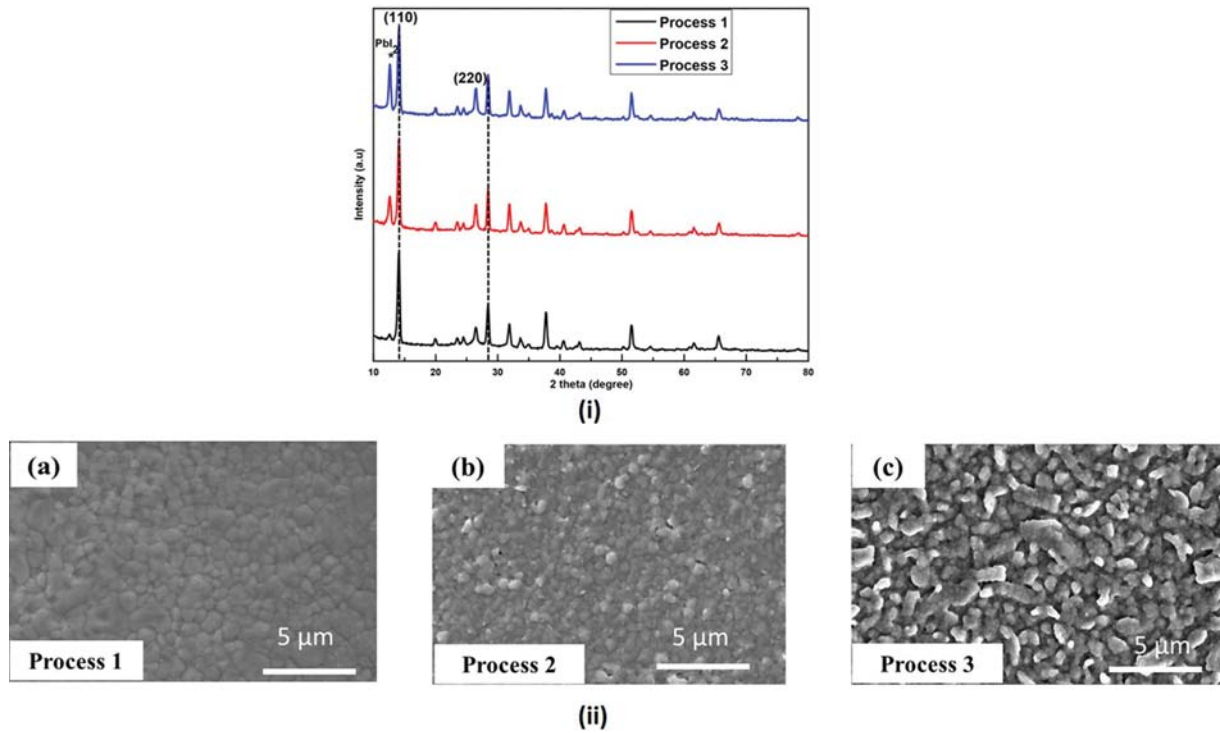Fig. 10. Three annealing methods for perovskite thin-films.

Fig. 11. XRD patterns and SEM images of perovskite thin-films at different annealing process.

ing process, the films were heated directly at 100 °C for 60 min and Fig. 10(c) shows the third annealing process; the films were heated in three steps (at 60 °C/15 min, 100 °C/30 min and 150 °C/15 min).

After annealing, the structural and morphological properties of the films were characterized using XRD and SEM (as shown in Fig. 11).

Fig. 11(i) shows the XRD pattern, which indicates that all the films have strong diffraction peaks at 14.14° and 28.43° corresponding to the planes (110) and (220) of perovskite thin films, respectively [32]. The PbI_2 diffraction peak at 12.6° indicates the existence of PbI_2 demonstrating the incomplete conversion from PbI_2 to $CH_3NH_3PbI_3$, which can reduce the performance of the cells [33]. The intensity of PbI_2 peak of the sample in the first annealing process is lower than the sample in the second and the third annealing process. In the second annealing process, heating the film immediately at 100 °C may cause too fast and uncontrollable evaporation of the solvent, which may result in an incomplete reaction and the film had many voids. In the third annealing process, when the reaction temperature reached 150 °C, $CH_3NH_3PbI_3$ decomposed into MAI and PbI_2, which was confirmed by a higher unreacted PbI_2 peak. However, in the first annealing process, the XRD pattern shows the smallest of PbI_2 peak. This can be explained by the slow solvent evaporation that leads to an increase in the reaction time between two precursors. The temperature was held at 60 °C for 15 min, leading to the evaporation of the solvent slower and MAI had more time to penetrate into the thick PbI_2 layer.

Fig. 11(ii) shows the morphology of the samples after annealing. In the first annealing process, the surface morphology of the sample is more uniform with higher coverage compared with the samples in the second and third annealing process. From the obtained results, we selected the first annealing process (at 60 °C/15 min and 100 °C/45 min) as the optimized condition for the fabrication of the device.

The devices of PVSCs at different annealing process were fabricated and characterized (shown in Fig. 12 and Table 3). The maxi-
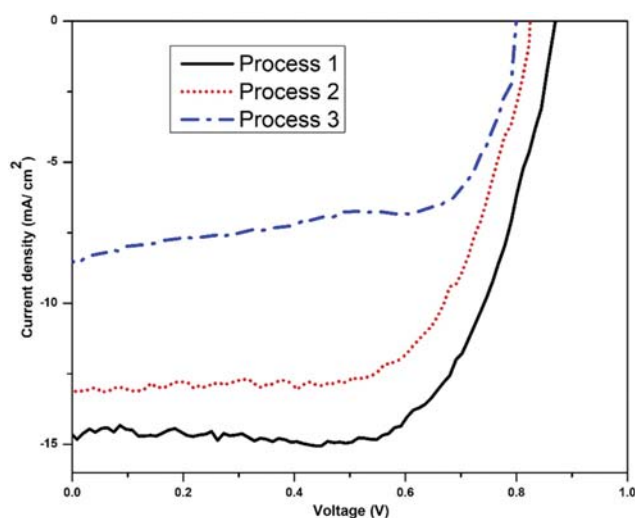
Table 3. Photovoltaic current-voltage parameters of perovskite solar cells at different annealing process

Samples	V_{oc} (V)	J_{sc} (mA/cm²)	FF (%)	PCE (%)
Process 1	0.87	14.64	67.7	8.6
Process 2	0.82	13.08	64.5	6.9
Process 3	0.80	8.49	64.5	4.4

mum power conversion efficiency of the fabricated device is about 8.6% (J_{sc} ~14.64 mA/cm²; V_{oc} ~0.87 V; FF ~67.7%). Our results show that the slow evaporation process can improve the quality of perovskite films, leading to increase the PCE of the device.

CONCLUSIONS

The effects of blending solvents and thermal annealing on the CH_3NH_3I active layer's properties were investigated. In this procedure, the results showed that the efficiency of perovskite solar cells could be enhanced by adding a volume of 25% 2-BTA solvent and optimizing the annealing temperature. Device parameters such as Jsc, Voc, FF, and efficiency were increased in comparison with the pristine device without optimization. The maximum power conversion efficiency is 8.6% (J_{sc} ~14.64 mA cm²; V_{oc} ~0.87 V; FF ~67.7%). The enhancement of device performance by optimization of HTL and ETL will be studied and reported in further work.

ACKNOWLEDGEMENTS

REFERENCES

1. T. J. Jacobsson, J.-P. Correa-Baena, M. Pazoki, M. Saliba, K. Schenk, M. Grätzel and A. Hagfeldt, *Energy Environ. Sci.*, **9**, 1706 (2016).
2. N. G. Park, M. Grätzel, T. Miyasaka, K. Zhu and K. Emery, *Nat. Energy*, **1**, 16152 (2016).
3. W. Deng, Z. Yuan, S. Liu, Z. Yang, J. Li, E. Wang, X. Wang and J. Li, *J. Power Sources*, **432**, 112 (2019).
4. K. Galkowski, A. Mitioglu, A. Miyata, P. Plochocka, O. Portugall, G. E. Eperon, J. T. W. Wang, T. Stergiopoulos, S. D. Stranks, H. J. Snaith and R. J. Nicholas, *Energy Environ. Sci.*, **9**, 962 (2016).
5. K. S. Anuratha, H. S. Peng, Y. Xiao, T. S. Su, T. C. Wei and J. Y. Lin, *Electrochim. Acta*, **295**, 662 (2019).
6. Y. Ogomi, A. Morita, S. Tsukamoto, T. Saitho, N. Fujikawa, Q. Shen, T. Toyoda, K. Yoshino, S. S. Pandey, T. Ma and S. Hayase, *J. Phys. Chem. Lett.*, **5**, 1004 (2014).
7. J. H. Im, H. S. Kim and N. G. Park, *APL Mater.*, **2**, 081510 (2014).
8. J. H. Im, C. R. Lee, J. W. Lee, S. W. Park and N. G. Park, *Nanoscale*, **3**, 4088 (2011).
9. A. Kojima, K. Teshima, Y. Shirai and T. Miyasaka, *J. Am. Chem. Soc.*, **131**, 6050 (2009).

Fig. 12. Current density-voltage (J-V) curves of perovskite films prepared at different annealing process.

10. Y. Hou, E. Aydin, M. De Bastiani, C. Xiao, F. H. Isikgor, D. J. Xue, B. Chen, H. Chen, B. Bahrami, A. H. Chowdhury, A. Johnston, S. W. Baek, Z. Huang, M. Wei, Y. Dong, J. Troughton, R. Jalmood, A. J. Mirabelli, T. G. Allen, E. V. Kerschaver, M. I. Saidaminov, D. Baran, Q. Qiao, K. Zhu, S. De Wolf and E. H. Sargent, *Science*, **367**, 1135 (2020).

11. X. Sun, C. Zhang, J. Chang, H. Yang, H. Xi, G. Lu, D. Chen, Z. Lin, X. Lu, J. Zhang and Y. Hao, *Nano Energy*, **28**, 417 (2016).

12. M. M. Lee, J. Teuscher, T. Miyasaka, T. N. Murakami and H. J. Snaith, *Science*, **338**, 643 (2012).

13. V. Arivazhagan, J. Xie, Z. Yang, P. Hang, M. M. Parvathi, K. Xiao, C. Cui, D. Yang and X. Yu, *Sol Energy*, **181**, 339 (2019).

14. Q. Chen, H. Zhou, Z. Hong, S. Luo, H. S. Duan, H. H. Wang, Y. Liu, G. Li and Y. Yang, *J. Am. Chem. Soc.*, **136**, 622 (2014).

15. T. T. Duong, P. H. Hoang, L. T. Nhan, L. V. Duong, M. H. Nam and L. Q. Tuan, *Curr. Appl. Phys.*, **19**, 1266 (2019).

16. X. Peng, J. Yuan, S. Shen, M. Gao, A. S. R. Chesman, H. Yin, J. Cheng, Q. Zhang and D. Angmo, *Adv. Funct. Mater.*, **27**, 1703704 (2017).

17. M. Wang, Y. Feng, J. Bian, H. Liu and Y. Shi, *Chem. Phys. Lett.*, **692** (2017).

18. K. L. Gardner, J. G. Tait, T. Merckx, W. Qiu, U. W. Paetzold, L. Kootstra, M. Jaysankar, R. Gehlhaar, D. Cheyns, P. Heremans and J. Poortmans, *Adv. Energy Mater.*, **6**, 1600386 (2016).

19. N. J. Jeon, J. H. Noh, Y. C. Kim, W. S. Yang, S. Ryu and S. I. Seok, *Nat. Mater.*, **13**, 897 (2014).

20. E. Guillén, F. J. Ramos, J. A. Anta and S. Ahmad, *J. Phys. Chem. C*, **118**, 22913 (2014).

21. J. H. Im, I. H. Jang, N. Pellet, M. Grätzel and N. G. Park, *Nat. Nanotechnol.*, **9**, 927 (2014).

22. D. Liu, J. Yang and T. L. Kelly, *J. Am. Chem. Soc.*, **136**, 17116 (2014).

23. H. Zhang, J. Mao, H. He, D. Zhang, L. Zhu, F. Xie, K. Wong, M. Grätzel and W. Choy, *Adv. Energy Mater.*, **5**, 1501354 (2015).

24. B. W. Park, N. Kedem, M. Kulbak, D. Lee, W. Yang, N. Jeon, J. Seo, G. Kim, K. Kim, T. Shin, G. Hodes, D. Cahen and S. I. Seok, *Nat. Commun.*, **9**, 3301 (2018).

25. T. P. Gujar, T. Unger, A. Schönleber, M. Fried, F. Panzer, S. van Smaalen, A. Köhler and M. Thelakkat, *Phys. Chem. Chem. Phys.*, **20**, 605 (2018).

26. G. Li, T. Zhang and Y. Zhao, *J. Mater. Chem. A*, **3**, 19674 (2015).

27. Y. Shi, X. Wang, H. Zhang, B. Li, H. Lu, T. Ma and C. Hao, *J. Mater. Chem. A*, **3**, 22191 (2015).

28. C. H. Chiang, M. Nazeeruddin, M. Grätzel and C. G. Wu, *Energy Environ. Sci.*, **10**, 808 (2017).

29. L. Su, Y. Xiao, G. Han, L. Lu, H. Li and M. Zhu, *J. Power Sources*, **426**, 11 (2019).

30. T. Abzieher, F. Mathies, M. Hetterich, A. Welle, D. Gerthsen, U. Lemmer, U. W. Paetzold and M. Powalla, *Phys. Status Solidi A*, **214**, 1700509 (2017).

31. K. O. Kosmatos, L. Theofylaktos, E. Giannakaki, D. Deligiannis, M. Konstantakou and T. Stergiopoulos, *Energy Environ. Mater.*, **2**, 79 (2019).

32. Z. L. Tseng, C. H. Chiang and C. G. Wu, *Sci. Rep.*, **5**, 13211 (2015).

33. J. Barbé, M. Newman, S. Lilliu, V. Kumar, H. K. H. Lee, C. Charbonneau, C. Rodenburg, D. Lidzey and W. C. Tsoi, *J. Mater. Chem. A*, **6**, 23010 (2018).

34. S. Yang, Y. C. Zheng, Y. Hou, X. Chen, Y. Chen, Y. Wang, H. Zhao and H. G. Yang, *Chem. Mater.*, **26**, 6705 (2014).

35. Y. Fu, F. Meng, M. B. Rowley, B. J. Thompson, M. J. Shearer, D. Ma, R. J. Hamers, J. C. Wright and S. Jin, *J. Am. Chem. Soc.*, **137**, 5810 (2015).

36. T. T. T. Le, N. Le, M. R. Pallavolu, Y. Jeon, D. S. Jeong, B. Pejjai, V. R. M. Reddy, N. T. N. Truong and C. Park, *Korean J. Chem. Eng.*, **36**, 2110 (2019).

37. L. C. Chen, J. C. Chen, C. Cheng-Chiang and C. G. Wu, *Nanoscale Res. Lett.*, **10**, 1020 (2015).